Research Article

Journal of Environmental Nanotechnology

Development and Characterization of ACV-Zn@PVP Nanoparticles for In Vitro Antibacterial and Cytotoxic Applications

Deva Dharshnini[1], Gulipalli Pallavi[2] and Sorimuthu Revathi[3]*

[1]MBBS 4st year, Saveetha Medical College and Hospital, Saveetha Institute of Medical and Technical Sciences, Chennai, TN, India

[2]MD General Medicine 3rd year, Saveetha Medical College and Hospital, Saveetha Institute of Medical and Technical Sciences, Chennai, TN, India

[3]Department of Emergency Medicine, Saveetha Medical College and Hospital, Saveetha Institute of Medical and Technical Sciences, Chennai, TN, India

Received: 19.07.2026 Accepted: 10.08.2026 Published: xx.xx.xxxx

*revathis1598@gmail.com

ABSTRACT

The increasing prevalence of multidrug-resistant (MDR) bacterial infections necessitates the development of novel, biocompatible antimicrobial nanomaterials. In the present study, *Adiantum capillus-veneris*-functionalized polyvinylpyrrolidone (PVP)-coated zinc oxide nanoparticles (ACV-Zn@PVP NPs) were successfully synthesized using a simple one-pot green synthesis approach. The aqueous leaf extract of ACV served as a natural reducing and capping agent, while PVP acted as a stabilizing polymer to improve nanoparticle dispersion and colloidal stability. The synthesized NPs were characterized using UV–Visible spectroscopy, FTIR, FESEM–EDX, XRD, DLS, and zeta potential analysis. UV–Vis spectra confirmed ACV-Zn@PVP NP formation with an absorption peak at 370 nm. XRD analysis revealed a highly crystalline hexagonal wurtzite ZnO structure with an average crystallite size of 22–25 nm. DLS analysis showed a Z-average hydrodynamic diameter of 219.7 nm with a polydispersity index (PDI) of 0.2888, while the zeta potential of −18.61 mV indicated moderately good colloidal stability. FESEM showed predominantly spherical NPs with reduced aggregation. EDX confirmed the presence of Zn and O as the elements, whereas DLS and zeta potential analyses indicated nanoscale particle size and good colloidal stability. The synthesized ACV-Zn@PVP NPs exhibited concentration-dependent antibacterial activity against *Escherichia coli*, *Staphylococcus aureus*, *Pseudomonas aeruginosa*, and *Klebsiella pneumoniae*, with the maximum inhibition zone of 35 mm against *E. coli* at 100 mg/mL. Cytocompatibility studies using V79 fibroblast cells showed 95% cell viability at 10 µg/mL, which gradually decreased to 69% at 160 µg/mL, indicating dose-dependent cytotoxicity while maintaining acceptable cellular compatibility at lower concentrations. Overall, the synthesized ACV-Zn@PVP NPs exhibited excellent characteristics, potent antibacterial activity, and cytocompatibility, highlighting their potential as promising multifunctional nanomaterials for future biomedical applications.

Keywords: *Adiantum capillus-veneris*; Zinc oxide nanoparticles; Polyvinylpyrrolidone; Green synthesis; Nanobiotechnology; Medicine.

1. INTRODUCTION

The rapid emergence of multidrug-resistant (MDR) bacterial pathogens has become one of the most significant global public health challenges and substantially limits the effectiveness of conventional antibiotic therapies (Ahmed *et al.* 2024). The excessive use of antibiotics has accelerated the evolution of resistant bacterial strains, prolonged infections, healthcare costs, and higher mortality rates. Consequently, the development of novel antimicrobial agents with improved efficacy, enhanced biocompatibility, and reduced toxicity has become an important area of biomedical research (Elshobary *et al.* 2025; Salam *et al.* 2023). In recent years, nanotechnology has emerged as a promising strategy for combating antimicrobial resistance by enabling the development of multifunctional nanomaterials with unique physicochemical and biological properties. Among various metal oxide nanomaterials, zinc oxide nanoparticles (ZnO NPs) have attracted considerable attention due to their broad-spectrum antibacterial activity, chemical stability, excellent biocompatibility, and cost-effective synthesis (Parvin *et al.* 2025; Pathak *et al.* 2026). ZnO NPs exert antimicrobial effects through many mechanisms, including the generation of ROS, disruption of bacterial cell membranes, leakage of intracellular components, and release of Zn^{2+} ions that interfere with essential cellular metabolic pathways. Their antibacterial properties, ZnO NPs have demonstrated cytotoxic effects against cancer cells, making them attractive candidates for biomedical applications such as antimicrobial coatings, drug delivery systems, wound healing, tissue engineering, and anticancer therapy (Sirelkhatim *et al.* 2015). However, conventional chemical synthesis methods often require hazardous reducing agents and stabilizers, raising concerns regarding environmental safety and biological

compatibility. Green synthesis using medicinal plant extracts has emerged as an environmentally friendly and sustainable alternative to conventional NPs synthesis (Dheyab *et al.* 2025). Plant-derived compounds serve simultaneously as reducing, capping, and stabilizing agents, eliminating the need for toxic chemicals while improving nanoparticle stability and biological activity (Villagrán *et al.* 2024). Moreover, bioactive compounds functionalized NPs frequently exhibit enhanced antimicrobial, antioxidant, anti-inflammatory, and anticancer activities because of the synergistic interaction between the bioactive plant compounds and the metallic nanostructures. Therefore, plant-based synthesis has become an increasingly attractive approach for the fabrication of multifunctional nanomaterials intended for biomedical applications (Diab *et al.* 2025).

Adiantum capillus-veneris (ACV), commonly known as the maidenhair fern, is a medicinal plant widely distributed in tropical and subtropical regions. Traditionally, it has been used in various systems of medicine for the treatment of respiratory disorders, fever, urinary tract infections, skin diseases, and inflammatory conditions(Qadir *et al.* 2025). Bioactive compounds have been investigated, revealing that ACV contains a rich diversity of compounds, including flavonoids, phenolic acids, triterpenoids, tannins, saponins, alkaloids, glycosides, and carotenoids(Dehdari and Hajimehdipoor, 2018). These secondary metabolites possess potent antioxidant, antimicrobial, anti-inflammatory, antiviral, and anticancer activities and are capable of reducing metal ions while simultaneously stabilizing the NPs. Consequently, ACV represents an excellent natural resource for the green synthesis of functionalized metal oxide NPs with improved biomedical performance (Nazim *et al.* 2018).

Although numerous studies have reported the green synthesis of ZnO nanoparticles using different medicinal plants, important limitations remain regarding nanoparticle aggregation, colloidal instability, and inconsistent biological performance, which significantly restrict their biomedical applications(El-Saadony *et al.* 2024; Surya *et al.* 2026). Furthermore, most previous investigations have focused either on plant-mediated ZnO nanoparticles or polymer-coated ZnO nanoparticles individually, whereas studies integrating medicinal plant phytochemicals with polymer-functionalized ZnO nanoparticles remain limited. In particular, despite the well-documented pharmacological properties of *Adiantum capillus-veneris*, including its antioxidant, antimicrobial, anti-inflammatory, and wound-healing activities, its application as both a bioreducing and biofunctionalizing agent for PVP-coated ZnO nanoparticles has not been comprehensively explored (Qadir *et al.* 2025). This represents a significant research gap because the synergistic interaction between ACV phytochemicals, ZnO nanoparticles, and a biocompatible polymer coating may substantially improve nanoparticle stability and biological performance. Furthermore, only a limited number of studies have systematically correlated the physicochemical characteristics of polymer-functionalized green ZnO nanoparticles with their antibacterial efficacy and cytocompatibility, thereby restricting their translational potential for biomedical applications.

Although green-synthesized ZnO NPs have demonstrated promising biological activities, NP aggregation remains a major limitation that adversely affects their stability, dispersion, and biological efficiency (Kiran and Kumar, 2026; Vantipalli *et al.* 2024). Surface modification using biocompatible polymers has therefore become an effective strategy to improve NP performance (Ragavendran *et al.* 2025; Sayeem *et al.* 2026). PVP is one of the most extensively used polymeric stabilizers because of its excellent water solubility, low toxicity, high biocompatibility, and strong metal-binding capability. PVP forms a protective coating around ZnO NP, thereby minimizing aggregation, enhancing colloidal stability, improving dispersion, and increasing the active surface sites responsible for biological interactions(Franco and De Marco, 2020; Teodorescu and Bercea, 2015).

Among the various polymeric stabilizers reported for nanoparticle synthesis, including polyethylene glycol (PEG), chitosan, polyvinyl alcohol (PVA), and poly(vinyl pyrrolidone) (PVP), PVP offers several distinct advantages. Unlike chitosan, whose solubility is pH-dependent and may exhibit batch-to-batch variability, PVP possesses excellent water solubility over a wide pH range and forms highly stable colloidal dispersions(AboGabal *et al.* 2023; Harun-Ur-Rashid *et al.* 2025; Ramnandan *et al.* 2021). Compared with PEG, PVP provides stronger coordination through its carbonyl groups, resulting in improved steric stabilization, reduced nanoparticle aggregation, enhanced surface uniformity, and better long-term colloidal stability. In addition, PVP is non-toxic, non-immunogenic, highly biocompatible, and widely accepted for pharmaceutical and biomedical applications, making it an ideal polymer for surface functionalization of ZnO nanoparticles. These characteristics make PVP one of the most frequently employed polymers for stabilizing metal oxide nanoparticles intended for biological applications. Therefore, combining PVP with phytochemical-mediated synthesis provides a rational strategy to simultaneously improve nanoparticle stability and biological activity.

Based on these considerations, the novelty of the present study lies in the development of a green-synthesized *Adiantum capillus-veneris*-functionalized PVP-coated ZnO nanocomposite (ACV-Zn@PVP) through a simple one-pot synthesis approach. To the best of our knowledge, very few reports describe the combined use of A. capillus-veneris phytochemicals and

PVP for the fabrication of ZnO nanocomposites, followed by a systematic evaluation of their physicochemical properties, antibacterial activity against clinically relevant bacterial pathogens, and cytocompatibility using V79 fibroblast cells. Therefore, this study aimed to synthesize ACV-Zn@PVP nanocomposites, characterize their structural and physicochemical properties using UV–Visible spectroscopy, FTIR, FESEM-EDX, XRD, DLS, and zeta potential analyses, and evaluate their in vitro antibacterial efficacy and cytocompatibility to assess their potential as environmentally sustainable antimicrobial nanomaterials. The findings are expected to provide valuable insights into the development of stable, eco-friendly ZnO-based nanocomposites for future antimicrobial and biomedical applications.

2. MATERIALS AND METHODS

2.1 Materials

Zinc acetate dihydrate [$Zn(CH_3COO)_2 \cdot 2H_2O$] (≥99.9% purity) and poly(vinyl pyrrolidone) (PVP) were purchased from HiMedia Laboratories Pvt. Ltd. Ethanol (99.9% analytical grade) and distilled water (DW) were used throughout the study. Fresh *Adiantum capillus-veneris* plants were obtained from a commercially available nursery.

2.2 Preparation of *Adiantum capillus-veneris* Aqueous Extract

Fresh leaves of ACV were collected, thoroughly washed with running tap water followed by distilled water(DW) to remove dust and surface contaminants, and shade-dried at room temperature for 7–10 days. The dried leaves were pulverized into a fine powder using a laboratory grinder. Approximately 10g of the powdered was mixed with 100 mL of DW and heated at 70°C for 30 min under continuous stirring. The extract mixture was allowed to cool to room temperature and filtered through Whatman No. 1 filter paper. The obtained aqueous extract was stored at 4°C until further used as the reducing and stabilizing agent for NPs (Baliyan *et al.* 2022).

2.3 Green Synthesis of *Adiantum capillus-veneris*-functionalized PVP-Coated Zinc Oxide Nanoparticles (ACV-Zn@PVP NPs)

The ACV-Zn@PVP NPs were synthesized through a one-pot green synthesis approach (Unni *et al.* 2023) as illustrated in Fig. 1. Initially, 0.063 M zinc acetate dihydrate was dissolved in DW to prepare the precursor solution. Subsequently, 0.5 g of PVP was added to the zinc precursor solution and stirred continuously until completely dissolution. Thereafter, 20 mL of ACV extract was added dropwise into the reaction mixture under continuous magnetic stirring at 70°C. The reaction mixture was maintained under constant stirring for approximately 2 h, during which the solution gradually changed from pale brown to creamy white, indicating the formation of ZnO nanoparticles. The phytochemicals present in the ACV extract served as natural reducing and capping agents, while PVP acted as a stabilizing polymer to minimize nanoparticle aggregation and promote uniform particle growth. The synthesized nanoparticles were collected by centrifugation at 10,000 rpm for 15 min, washed three times with distilled water followed by ethanol to remove residual impurities, and dried in a hot-air oven at 60 °C overnight. The dried ACV-Zn@PVP nanoparticle powder was stored in airtight containers for subsequent physicochemical characterization and biological investigations.

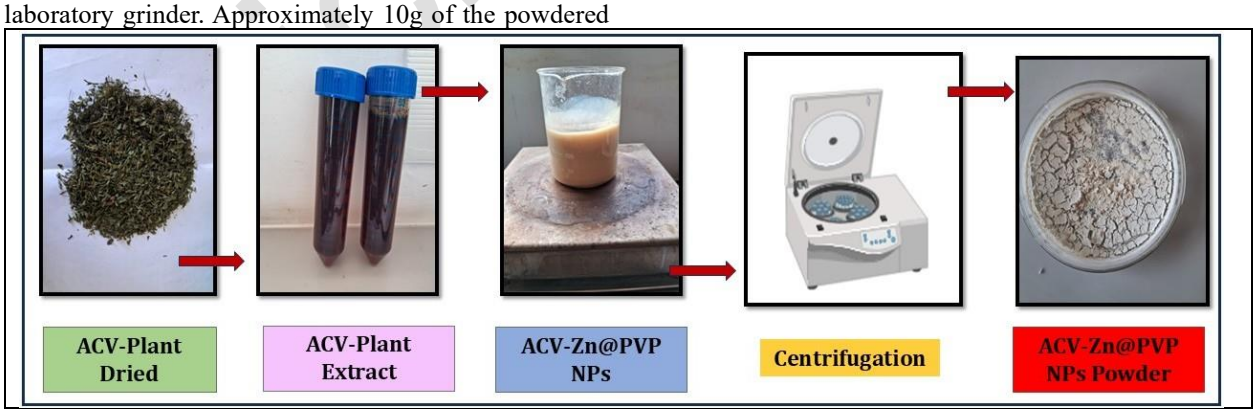

Fig. 1: Schematic representation of the green synthesis of ACV-Zn@PVP nanoparticles

2.4 Characterization of ACV-Zn@PVP Nanoparticles

2.4.1 UV–Visible Spectroscopy

The optical properties and nanoparticle formation were confirmed using a Lambda UV–Visible spectrophotometer (Alanazi, 2025). The absorbance spectra of the NPs were recorded over the wavelength range of 200–800 nm using DW as the reference blank.

The characteristic absorption peak confirmed the successful synthesis of ZnO NPs.

2.4.2 FTIR Spectroscopy

The functional groups responsible for NP and stabilization were analyzed using a PerkinElmer Spectrum Two FTIR spectrometer (Ali *et al.* 2025). The dried NP powder was mixed with potassium bromide (KBr) and compressed into pellets. Spectra were recorded within the range of 4000–400 cm^{-1} at room temperature. The obtained spectra were used to identify phytochemical functional groups involved in reduction, capping, and stabilization of ZnO NPs.

2.4.3 XRD Analysis

The crystalline structure and phase purity of ACV-Zn@PVP NPs were determined using an X-ray diffractometer (Bruker D8 Advance) equipped with Cu-Kα radiation (λ = 1.5406 Å). Diffraction patterns were recorded over a 2θ range of 20–80° at a scanning rate of 2° min^{-1} (Suciyati *et al.* 2024). The average crystallite size was estimated using the Debye–Scherrer equation.

$$D = \frac{0.9\lambda}{\beta \cos\ \theta}$$

where D is crystallite size, λ is X-ray wavelength, β is full width at half maximum (FWHM), and θ is Bragg's diffraction angle.

2.4.4 SEM and EDX Analysis

The surface morphology of the synthesized nanoparticles was examined using FESEM, JSM-IT800SHL. Prior to imaging, the dried NP powder was mounted onto carbon adhesive tape and sputter-coated with a thin layer of gold to improve conductivity. Images were captured at different magnifications to evaluate particle morphology and aggregation. Elemental composition was simultaneously analysed using an EDX detector attached to the FESEM instrument. The presence of zinc, oxygen, carbon, and other elemental constituents confirmed the successful synthesis and functionalization of the NPs(Santhoshkumar *et al.* 2017).

2.4.5 DLS and Zeta Potential Analysis

The hydrodynamic particle size distribution and surface charge of ACV-Zn@PVP nanoparticles were measured using a Malvern Panalytical Zetasizer (Olejnik *et al.* 2021). The NP suspension was prepared by dispersing the dried NPs in deionized water followed by ultrasonication for 15 min to ensure homogeneous dispersion. Particle size measurements were carried out using the dynamic light scattering principle, whereas zeta potential analysis was performed by electrophoretic light scattering to determine colloidal stability. Each measurement was performed in triplicate, and the average values were reported.

2.5 Biomedical Applications

2.5.1 Antibacterial Activity

The antibacterial activity of ACV-Zn@PVP NPs was evaluated by the agar well diffusion method against both Gram-positive and Gram-negative bacterial strains, including *Staphylococcus aureus*, *Escherichia coli*, *Pseudomonas aeruginosa*, and *Klebsiella pneumoniae* (Yagnik *et al.* 2018). Fresh bacterial cultures were adjusted to approximately 0.5 McFarland standard (1.5×10^8 CFU/mL) and uniformly spread onto Mueller–Hinton agar plates using sterile cotton swabs. Wells of 6 mm diameter were punched aseptically into the agar medium. Different concentrations of ACV-Zn@PVP NPs (25, 50, and 100 mg/mL) were prepared in sterile DW, and 100 µL of each concentration was added into the respective wells. Amoxicillin served as the positive control. The plates were incubated at 37°C for 24 h, after which the zone of inhibition (mm).

2.5.2 In Vitro Cytotoxicity Assay

The cytotoxicity of ACV-Zn@PVP NPs was evaluated using the MTT assay on V79 (Chinese hamster lung fibroblast) cells (Namvar *et al.* 2015). V79 cells were cultured in Dulbecco's Modified Eagle Medium (DMEM) supplemented with 10% fetal bovine serum (FBS), 100 U/mL penicillin, and 100 µg/mL streptomycin under standard incubation conditions (37°C, 5% CO_2, and 95% humidity). Cells were seeded into 96-well plates at a density of 1×10^4 cells/well and allowed to attach overnight. The culture medium was then replaced with fresh medium containing ACV-Zn@PVP NPs at concentrations of 6.25, 12.5, 25, 50, and 100 µg/mL. Untreated cells served as the control. Following 24 h incubation, 20 µL of MTT solution (5 mg/mL) was added to each well and incubated for 4 h. The resulting purple formazan crystals were dissolved using 100 µL of dimethyl sulfoxide (DMSO), and absorbance was measured at 570 nm using a microplate reader. Cell viability (%) was calculated using the following equation:

$$\text{Cell viability (\%)} = \frac{\text{Absorbance of treated cells}}{\text{Absorbance of control cells}} \times 100$$

All experiments were performed in triplicate, and the results were expressed as mean ± standard deviation. The IC_{50} value was calculated using GraphPad Prism software.

3. RESULTS AND DISCUSSION

3.1 UV–Visible Spectral Analysis of ACV-Zn@PVP Nanoparticles

The formation of ACV-Zn@PVP nanoparticles was initially confirmed by UV–Visible spectroscopy, and the corresponding spectra are presented in Fig. 2. The aqueous extract of ACV exhibited an absorption peak at 307 nm, which is attributed to the presence of phenolic compounds, flavonoids, and other phytocompounds in the plant extract. Following the addition of the zinc precursor and PVP, a distinct absorption peak was observed at 370 nm, confirming the successful formation of ZnO NPs. The absorption band corresponds to the intrinsic band gap excitation of ZnO, arising from electron transitions between the valence and conduction bands and is characteristic of nanosized ZnO.

The observed red shift from 307 to 370 nm indicates the reduction of Zn^{2+} ions by the action ACV phytochemicals and reflects a change in the electronic structure associated with NP nucleation and crystal growth (Ansari *et al.* 2020; Ihsan *et al.* 2023). The shift toward a longer wavelength can be attributed to increased particle crystallinity, surface functionalization by phytochemicals, and the coordination of PVP molecules with the nanoparticle surface, which modifies the local dielectric environment and reduces surface defect states. In addition, the interaction between the carbonyl groups of PVP and Zn^{2+} ions provides steric stabilization during nanoparticle growth, resulting in controlled nucleation and improved optical properties.

The sharp and well-defined absorption peak with the absence of additional broad bands suggests a narrow particle size distribution and reduced nanoparticle aggregation. The PVP coating effectively prevented particle agglomeration by forming a protective polymer layer around the ZnO nanoparticles, thereby improving colloidal stability. Similar absorption peaks around 367–375 nm have been reported for PVP-coated ZnO NP, confirming that PVP improves NP stability without significantly altering the intrinsic optical properties of ZnO (Singh *et al.* 2023). Likewise, PVP-capped ZnO NPs exhibited enhanced UV emission and reduced defect-related visible emission due to surface passivation and decreased oxygen vacancies defects (Kim *et al.* 2019). Comparable UV absorption bands in the range of 360–380 nm have also been reported for plant-mediated ZnO NPs, demonstrating the effective role of phytochemicals in NP synthesis and stabilization (Abdolalian and Taghavijeloudar, 2022; Kazemi *et al.* 2023). Overall, the UV–Visible results confirmed the successful biosynthesis of stable ACV-Zn@PVP nanoparticles suitable for further characterization and biological evaluation.

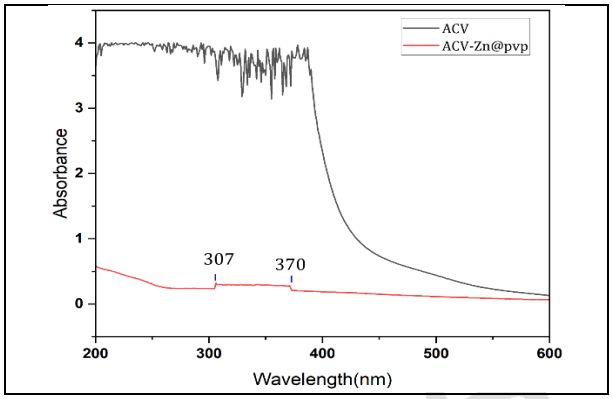

Fig. 2: UV–Visible absorption spectra of ACV aqueous extract and ACV-Zn@PVP nanoparticles

3.2 FTIR Spectral Analysis of ACV-Zn@PVP Nps

The chemical composition and functional groups involved in the biosynthesis and stabilization of ACV-Zn@PVP NPs were investigated using FTIR spectroscopy, and the spectrum is presented in Fig.3, while the corresponding peak assignments are summarized in Table 1. The broad absorption band observed at 3384 cm^{-1} corresponds to the stretching vibration of hydroxyl (O–H) groups, indicating the presence of phenolic compounds, flavonoids, and adsorbed water molecules derived from the ACV extract (Ibraheim *et al.* 2011; Omidi *et al.* 2018). The absorption peak at 2987 cm^{-1} is assigned to the asymmetric stretching vibration of aliphatic C–H groups, while the weak band at 1981 cm^{-1} may be associated with overtone or combination vibrations of organic functional groups. A prominent absorption band at 1661 cm^{-1} is attributed to the stretching vibration of the carbonyl (C=O) group of PVP, confirming the successful interaction between the polymer and ZnO NPs (Mesbah *et al.* 2021; Tu *et al.* 2008). The peak at 1567 cm^{-1} corresponds to C=C aromatic stretching and N–H bending vibrations originating from plant compounds and residual biomolecules adsorbed on the NP surface. The bands observed at 1416 cm^{-1} and 1342 cm^{-1} are assigned to C–N stretching and CH_2 bending vibrations, respectively, whereas the absorption peak at 1287 cm^{-1} represents C–N stretching of the pyrrolidone ring of PVP, demonstrating coordination between the polymer carbonyl groups and zinc ions during NP formation (Safo *et al.* 2019). Similar findings have been reported for PVP-coated ZnO NPs, where the band at 1288 cm^{-1} indicated chemical interaction between PVP and ZnO, while the peak around 1655 cm^{-1} confirmed the presence of the PVP carbonyl group (Kim *et al.* 2019). The absorption bands at 882 cm^{-1} and 688 cm^{-1} were attributed to aromatic C–H bending and Zn–O lattice vibrations, respectively. Notably, the strong band at 535 cm^{-1} corresponds to Zn–O stretching, confirming the successful formation of ZnO NPs. Similar Zn–O

vibrations have been reported within the 450–700 cm^{-1} region for PVP-coated ZnO nanostructures (Singh *et al.* 2023).

The FTIR spectrum further demonstrates the synergistic interaction between ACV phytochemicals and PVP during nanoparticle synthesis. Hydroxyl and phenolic groups present in flavonoids and phenolic acids of the ACV extract initially reduce Zn^{2+} ions to ZnO nuclei and subsequently adsorb onto the nanoparticle surface through hydrogen bonding and electrostatic interactions. Simultaneously, the carbonyl (C=O) groups of PVP coordinate with surface Zn atoms, forming a protective polymer shell around the nanoparticles (Jebahi *et al.* 2025; Thakur and Kaur, 2025). This dual surface functionalization enhances nanoparticle stability by preventing particle aggregation through steric hindrance while maintaining good colloidal dispersion. The combined action of plant phytochemicals and PVP therefore provides both chemical stabilization and surface passivation, contributing to improved nanoparticle stability and biological performance. Comparable FTIR profiles have been reported for plant-mediated ZnO nanoparticles, demonstrating the role of compounds as natural reducing and capping agents that enhance NP stability and biological activity (Abdolalian and Taghavijeloudar, 2022; Kazemi *et al.* 2023). Overall, FTIR analysis confirmed the successful synthesis and surface functionalization of ACV-Zn@PVP NP.

Table 1. FTIR peak assignments of ACV-Zn@PVP nanoparticles

Wavenumber (cm^{-1})	Functional Group	Assignment	Role in Nanoparticle Formation
3384	O–H	Hydroxyl stretching	Phenolics/flavonoids involved in reduction and stabilization
2987	C–H	Aliphatic C–H stretching	Organic biomolecules from ACV extract
1981	–	Overtone/combination band	Organic phytochemical residues
1661	C=O	Carbonyl stretching (PVP)	Coordination of PVP with ZnO nanoparticles
1567	C=C / N–H	Aromatic stretching and N–H bending	Plant phytochemicals adsorbed on nanoparticle surface
1416	C–N	C–N stretching	Organic compounds/PVP interaction
1342	CH_2	CH_2 bending vibration	PVP backbone vibration
1287	C–N	Pyrrolidone ring stretching	PVP–Zn coordination and nanoparticle stabilization
882	C–H	Aromatic C–H bending	Plant-derived aromatic compounds
688	Zn–O	Zn–O lattice vibration	Formation of ZnO crystal lattice
535	Zn–O	Zn–O stretching vibration	Confirmation of ZnO nanoparticle formation

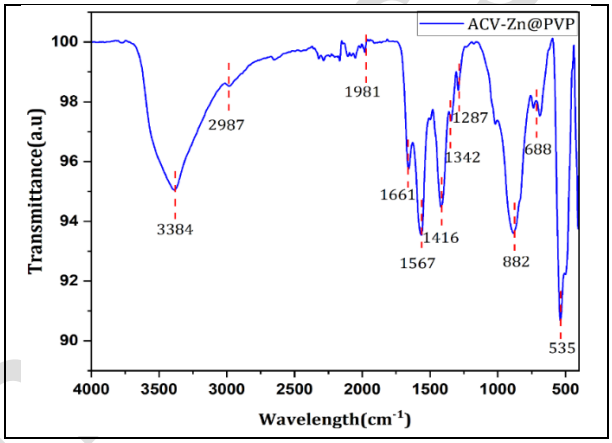

Fig. 3: FTIR spectrum of *Adiantum capillus-veneris*-functionalized PVP-coated zinc oxide nanoparticles

3.4 SEM and EDX Analysis of ACV-Zn@PVP NPs

The surface morphology and elemental composition of the synthesized ACV-Zn@PVP nanoparticles were investigated using FESEM coupled with EDX analysis, and results are presented in Fig.4(A–B). The FESEM image (Fig. 4A) revealed that the synthesized ACV-Zn@PVP NPs possessed predominantly quasi-spherical to spherical morphology with moderate agglomeration. The NPs were uniformly distributed, indicating that PVP effectively minimized particle aggregation by providing steric stabilization during NP growth. Based on FESEM image analysis, the nanoparticles exhibited an average particle size of approximately 43.4 nm, indicating successful nanoscale synthesis. The observed particle size was larger than the crystallite size obtained from XRD (22–25 nm), which is expected because FESEM measures the overall particle dimensions, whereas XRD estimates the coherent crystalline domain size. The rough and porous surface morphology is expected to increase the surface area available for interaction with bacterial cells, thereby enhancing the biological activity of the NPs. Similar observations have been reported for PVP-coated ZnO NPs, where PVP acted as an efficient capping agent to

control particle growth and improve morphological uniformity (Shanmugam *et al.* 2016). Comparable spherical ZnO NPs synthesized using medicinal plant extracts have also been reported, demonstrating the important role of phytochemicals in NP stabilization (Abdolalian and Taghavijeloudar, 2022; Kazemi *et al.* 2023).

The EDX spectrum (Fig. 4B) confirmed the elemental composition of the synthesized nanoparticles. Characteristic peaks corresponding to Zn, O, and C were observed, confirming the successful formation of PVP-functionalized ZnO nanoparticles. Quantitative elemental analysis showed 59.2 wt% C (39.0 at%), 22.9 wt% O (37.4 at%), and 17.9 wt% Zn (23.7 at%) (Table 2). The presence of the carbon signal originated from the PVP coating and residual phytochemicals adsorbed on the NP surface, while the Au peaks resulted from gold sputter coating during SEM sample preparation. No impurity peaks from other metallic elements were detected, indicating the high purity of the synthesized NPs. Similar elemental compositions have been reported for green-synthesized PVP-coated ZnO nanoparticles, confirming successful NP synthesis and effective surface functionalization (Shanmugam *et al.* 2016; Singh *et al.* 2023). Overall, the FESEM and EDX results confirmed the successful synthesis of uniformly distributed, high-purity ACV-Zn@PVP NPs with effective polymer coating, making them suitable for subsequent biomedical applications.

Table 2. Elemental composition of ACV-Zn@PVP nanoparticles determined by EDX

Element	Weight %	Atomic %
C	59.2	39.0
O	22.9	37.4
Zn	17.9	23.7

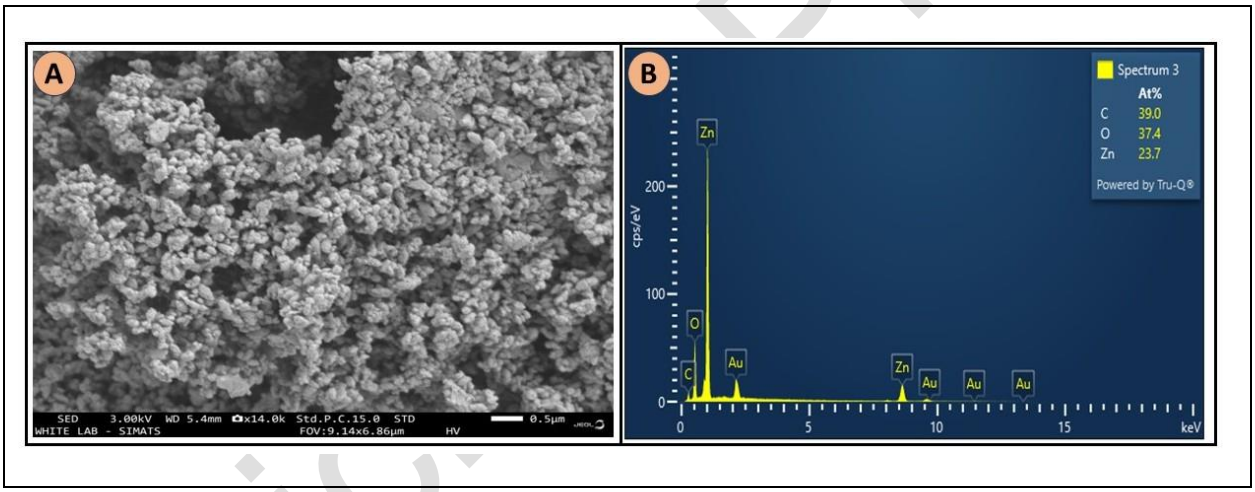

Fig. 4: (A) FESEM micrograph of ACV-Zn@PVP NPs and (B) EDX spectrum the elemental composition of the synthesized nanoparticles

3.5 XRD Analysis of ACV-Zn@PVP Nanoparticles

The crystalline structure and phase purity of the synthesized ACV-Zn@PVP NPs were investigated using XRD, and the obtained diffraction pattern is presented in (Fig.5). The diffraction peaks observed at 2θ = 31.85°, 34.55°, 36.36°, 47.70°, 56.75°, 63.09°, 68.17°, 69.29°, and 77.21° were indexed to the (100), (002), (101), (102), (110), (103), (112), (201), and (202) crystallographic planes, respectively, which correspond to the hexagonal wurtzite structure of ZnO (JCPDS Card No. 36-1451), confirming the successful formation of crystalline ZnO nanoparticles without secondary impurity phases. The absence of additional diffraction peaks further indicates the high phase purity of the synthesized nanocomposite.

The crystallite size was calculated using the Debye–Scherrer equation:

$$D = \frac{0.9\lambda}{\beta \cos\theta}$$

where D is the crystallite size, λ = 0.15406 nm (Cu Kα radiation), β is the full width at half maximum (FWHM) in radians, and θ is the Bragg diffraction angle. The average crystallite size was estimated to be 22–25 nm, confirming the formation of nanocrystalline ZnO. The relatively narrow diffraction peaks indicate good crystallinity, while the small crystallite size suggests that the phytochemicals present in *Adiantum capillus-veneris*, together with the PVP coating, effectively controlled crystal nucleation and growth during nanoparticle synthesis.

The lattice parameters calculated from the diffraction data were a = b ≈ 3.25 Å and c ≈ 5.21 Å, which closely agree with the standard hexagonal wurtzite ZnO structure (JCPDS No. 36-1451), confirming that neither the plant phytochemicals nor the PVP coating altered the intrinsic crystal lattice of ZnO. The calculated d-spacing values also showed excellent agreement with the corresponding standard JCPDS values, further verifying the successful formation of phase-pure ZnO nanoparticles. Similar diffraction patterns and crystallite sizes have been reported for PVP-coated ZnO NPs, confirming the formation of highly crystalline hexagonal ZnO with improved structural stability (Kim *et al.* 2019; Singh *et al.* 2023). Furthermore, recent studies on plant-mediated ZnO NPs have reported comparable XRD patterns, demonstrating that green synthesis produces phase-pure ZnO without altering its crystal structure (Abdolalian and Taghavijeloudar, 2022; Kazemi *et al.* 2023). Therefore, the XRD results confirm the successful synthesis of highly crystalline, phase-pure ACV–Zn@PVP nanoparticles suitable for subsequent biomedical applications.

Table 3. XRD parameters of ACV–Zn@PVP nanoparticles

2θ (°)	Plane (hkl)	Standard JCPDS 2θ (°)	d-spacing (Å)	FWHM (°) *	Crystallite Size (nm)
31.85	(100)	31.77	2.81	0.38	22.6
34.55	(002)	34.42	2.59	0.36	23.8
36.36	(101)	36.25	2.47	0.35	24.5
47.70	(102)	47.54	1.91	0.39	22.4
56.75	(110)	56.60	1.62	0.37	23.1
63.09	(103)	62.86	1.47	0.36	24.2
68.17	(112)	67.96	1.37	0.38	22.8
69.29	(201)	69.10	1.36	0.35	24.9
77.21	(202)	76.98	1.24	0.39	22.2

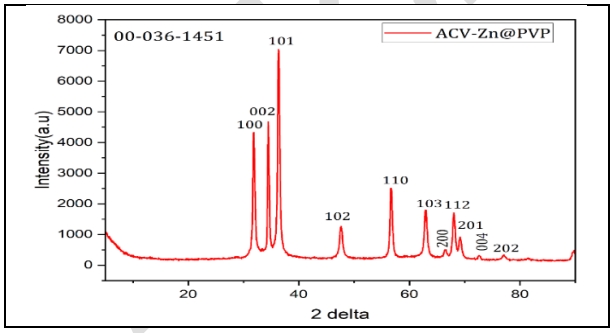

Fig. 5: XRD pattern of *Adiantum capillus-veneris*-functionalized PVP-coated zinc oxide nanoparticles

3.6 DLS and Zeta Potential Analysis of ACV-Zn@PVP Nanoparticles

The hydrodynamic particle size distribution and colloidal stability of the synthesized ACV-Zn@PVP NPs were evaluated using DLS and zeta potential analysis (Fig. 6A–B). The DLS analysis showed a Z-average hydrodynamic diameter of 219.7 nm with a polydispersity index (PDI) of 0.2888, indicating a moderately narrow particle size distribution and acceptable dispersion of the nanoparticles in aqueous medium. The PDI value below 0.3 suggests that the synthesized nanoparticles exhibit relatively uniform size distribution with limited aggregation, confirming the effectiveness of the green synthesis approach and PVP stabilization. The hydrodynamic diameter obtained by DLS was considerably larger than the average particle size observed by FESEM (~43.4 nm) and the crystallite size determined by XRD (22–25 nm). This difference is expected because DLS measures the hydrodynamic diameter of nanoparticles suspended in solution, including the surrounding hydration layer, adsorbed phytochemicals, and the PVP polymer coating, whereas FESEM measures the physical diameter of dried nanoparticles and XRD estimates only the crystalline domain size. Therefore, the larger DLS size does not indicate particle growth but rather reflects the hydrated state of the nanoparticles in suspension.

The zeta potential of the synthesized nanoparticles was measured to be −18.61 mV, indicating moderately good colloidal stability. The negative surface charge originates from the adsorption of hydroxyl, phenolic, and carboxyl-containing phytochemicals from *Adiantum capillus-veneris*, together with the carbonyl groups of the PVP coating. These surface functional groups provide both electrostatic repulsion and steric stabilization, thereby reducing nanoparticle aggregation and improving suspension stability. Although zeta potential values greater than ±30 mV are generally considered highly stable, polymer-coated nanoparticles frequently exhibit satisfactory stability at lower absolute zeta potential values because steric stabilization provided by PVP complements electrostatic repulsion (Karampour, 2023).

Similar observations have been reported for green-synthesized PVP-coated ZnO nanoparticles, where larger hydrodynamic diameters than microscopic particle sizes were attributed to hydration and polymer adsorption, while negative zeta potential values confirmed stable colloidal dispersions (Karampour, 2023; Kim *et al.* 2019). Likewise, (Karampour, 2023) reported green-synthesized ZnO nanoparticles with negative surface charge and good colloidal stability suitable for biomedical applications(Karampour, 2023). Overall, the DLS and zeta potential analyses demonstrate that ACV–Zn@PVP nanoparticles possess acceptable particle size distribution, moderate colloidal stability, and favorable dispersion characteristics for subsequent antibacterial and cytocompatibility studies. Overall, the DLS and zeta potential analyses demonstrate that ACV-Zn@PVP NP possess a uniform particle size distribution and excellent colloidal stability, making them suitable for subsequent antibacterial and cytotoxic applications.

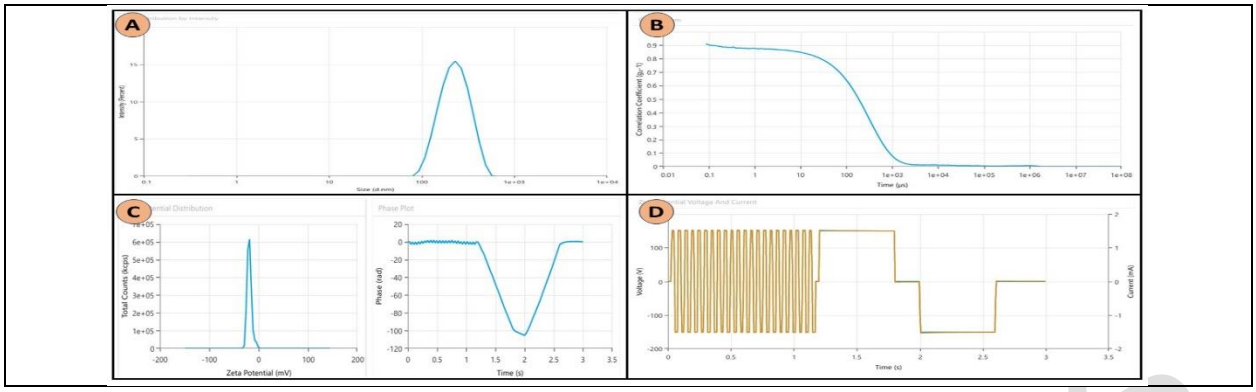

Fig. 6: (A) DLS analysis showing the hydrodynamic particle size distribution of ACV-Zn@PVP NPs and (B) Zeta potential analysis indicating the surface charge and colloidal stability of the synthesized nanoparticles

3.7 Antibacterial Activity of ACV-Zn@PVP Nanoparticles

The antibacterial activity of ACV-Zn@PVP NPs was evaluated against Gram-negative (*Escherichia coli*, *Pseudomonas aeruginosa*, and *Klebsiella pneumoniae*) and Gram-positive (*Staphylococcus aureus*) bacterial strains using the agar well diffusion assay Fig.7 and Fig. 8. Proposed antibacterial mechanism of ACV–Zn@PVP nanoparticles. The NPs exhibited concentration-dependent antibacterial activity against all tested pathogens. Among the bacterial strains, *E. coli* showed the highest susceptibility, with inhibition zones increasing from 21 mm at 25 mg/mL to 35 mm at 100 mg/mL, followed by K. pneumoniae from 25–30 mm. Moderate antibacterial activity was observed against P. aeruginosa from 17–20 mm, whereas S. aureus exhibited the lowest susceptibility from 11–15 mm. In comparison, the aqueous plant extract alone produced only moderate inhibition from 11–14 mm, demonstrating that NP formation significantly enhanced the antibacterial efficacy. The enhanced antibacterial activity of ACV–Zn@PVP nanoparticles can be attributed to the synergistic effects of ZnO nanoparticles, ACV phytochemicals, and the PVP coating. ZnO nanoparticles are known to exert antibacterial activity through multiple mechanisms, including the generation of reactive oxygen species (ROS), disruption of bacterial cell membranes, leakage of intracellular constituents, and the release of Zn^{2+} ions that interfere with essential metabolic enzymes and nucleic acid synthesis (Mohammed *et al.* 2025; Sirelkhatim *et al.* 2015). Simultaneously, the flavonoids, phenolic compounds, and triterpenoids present in *Adiantum capillus-veneris* contribute additional antibacterial activity by increasing membrane permeability, inhibiting bacterial enzymes, and suppressing microbial growth. Furthermore, the PVP coating improves nanoparticle dispersion, minimizes aggregation, and enhances nanoparticle–bacterial cell interactions, thereby increasing the effective antibacterial performance.

The present findings are in agreement with previous reports describing the antibacterial potential of *A. capillus-veneris* extracts against both Gram-positive and Gram-negative bacterial pathogens (Ebrahimzadeh *et al.* 2024; Irma *et al.* 2023; Ishaq *et al.* 2014). reported significant antibacterial activity of ACV extracts against clinically important bacterial species. Green-synthesized ZnO nanoparticles stabilized using medicinal plant extracts have likewise demonstrated concentration-dependent antibacterial activity through ROS-mediated oxidative stress and Zn^{2+} ion release (Abdolalian and Taghavijeloudar, 2022; Kazemi *et al.* 2023). The maximum inhibition zone observed for ACV–Zn@PVP nanoparticles against *E. coli* (35 mm) is comparable to or greater than several previously reported plant-mediated ZnO nanoparticles, indicating that the synergistic combination of ACV phytochemicals and PVP surface functionalization effectively enhances antibacterial performance. Overall, these findings demonstrate that ACV–Zn@PVP nanoparticles possess promising broad-spectrum antibacterial activity and may serve as environmentally friendly antimicrobial nanomaterials for future biomedical applications.

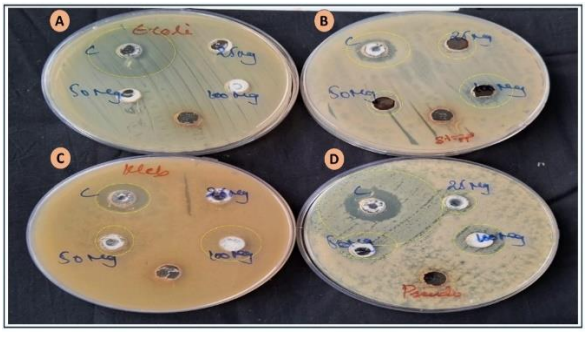

Fig. 7: Antibacterial activity of ACV-Zn@PVP NPs against various microorganisms determined by the agar well diffusion method

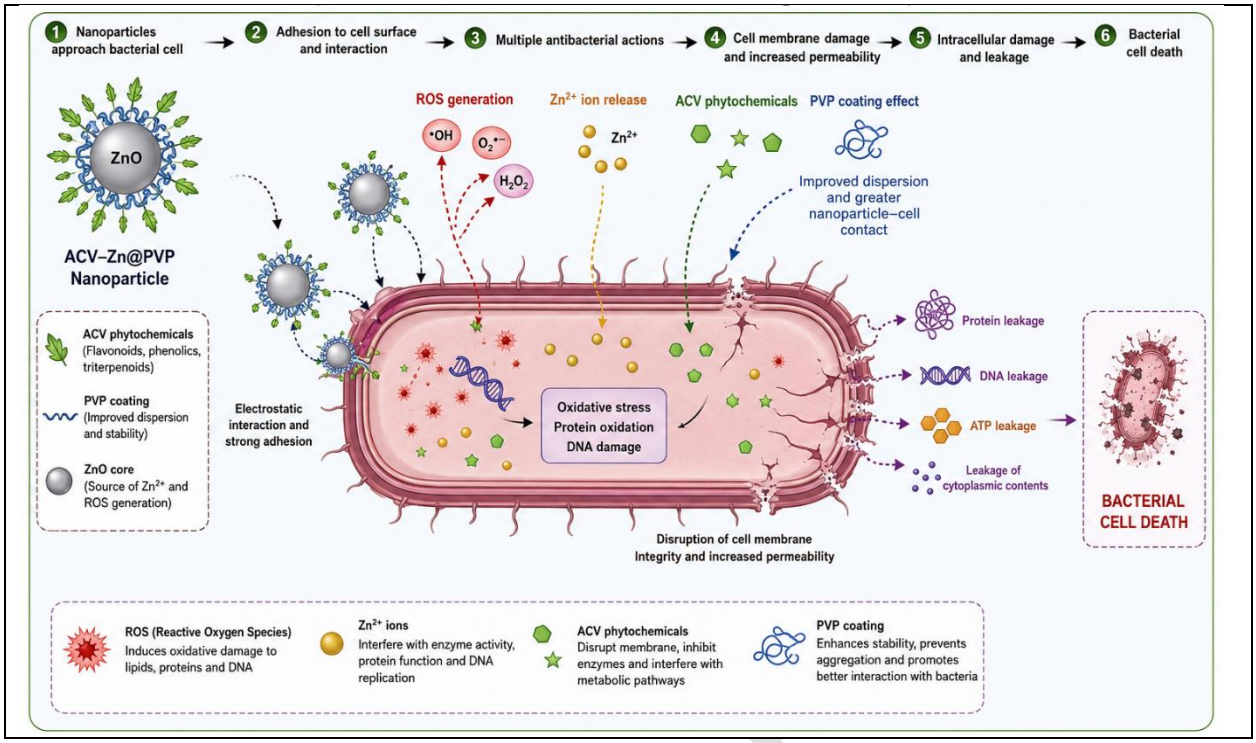

Fig. 8: Proposed antibacterial mechanism of ACV–Zn@PVP nanoparticles against bacterial pathogens

3.8 In Vitro Cytotoxicity of ACV-Zn@PVP Nanoparticles

The cytotoxicity of ACV-Zn@PVP NPs was evaluated against V79 fibroblast cells using the MTT assay, and the results are presented in Fig.8. The synthesized NPs exhibited a concentration-dependent reduction in cell viability. Untreated control cells showed nearly 100% viability, whereas cells treated with 10, 20, 40, 80, and 160 µg/mL retained approximately 95%, 91%, 88%, 77%, and 69% viability, respectively. Statistical analysis indicated that the observed reductions in cell viability were not statistically significant (ns; $p > 0.05$) compared with the untreated control under the experimental conditions. These findings indicate that ACV-Zn@PVP NPs possess good cytocompatibility at lower concentrations and moderate cytotoxicity at higher concentrations.

The moderate reduction in cell viability is mainly attributed to intracellular ROS generation and Zn^{2+} ion release from ZnO NPs, leading to oxidative stress and mitochondrial dysfunction. However, the PVP coating and ACV phytochemicals likely reduced excessive cellular damage by improving NP dispersion, minimizing aggregation, and enhancing biocompatibility. Similar dose-dependent cytotoxic effects of ZnO NPs have been reported by Pinho et al. 2020), who demonstrated that ROS-mediated oxidative stress was the primary mechanism responsible for reduced cell viability. Likewise, ACV extracts have shown concentration-dependent cytotoxic activity against HeLa and other human cancer cell lines, indicating the presence of bioactive compounds with antiproliferative potential (Roy *et al.* 2019). Overall, the moderate cytotoxicity observed toward normal V79 fibroblast cells suggests that ACV-Zn@PVP NPs possess cellular safety while retaining promising potential for future antimicrobial and biomedical applications.

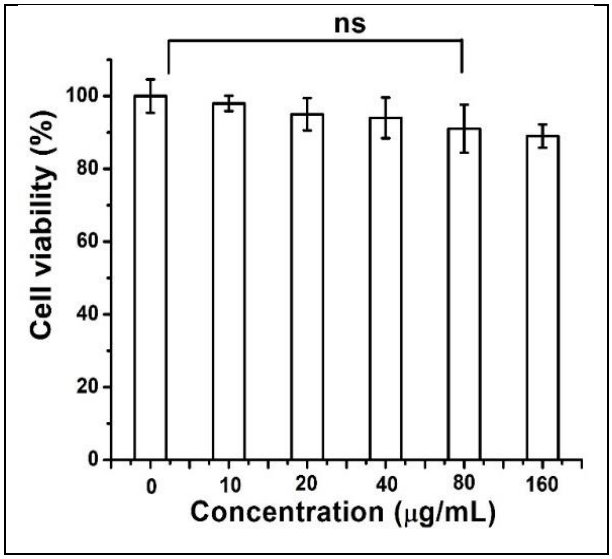

Fig. 8: In vitro cytocompatibility of ACV-Zn@PVP nanoparticles against V79 fibroblast cells determined by the MTT assay after 24 h of exposure

Cells were treated with ACV-Zn@PVP nanoparticles at concentrations of 6.25, 12.5, 25, 50, and

100 µg/mL. Data are presented as mean ± SD (n = 3). Statistical significance was determined using one-way ANOVA followed by Tukey's post hoc test ($p < 0.05$).

3.9 Morphological Evaluation of V79 Cells of ACV-Zn@PVP Nanoparticle Treatment

The morphological changes induced by ACV-Zn@PVP NPs in V79 fibroblast cells were examined by phase-contrast microscopy after 24 h of exposure, and the representative images are presented in Fig. 9. Untreated control cells exhibited a typical spindle-shaped fibroblast morphology with intact plasma membranes and strong adherence to the culture surface. Cells treated with 10 and 20 µg/mL maintained normal morphology with only minimal changes, indicating good cytocompatibility at lower concentrations. Mild morphological alterations, including slight cell shrinkage and reduced cell spreading, were observed at 40 µg/mL. At higher concentrations (80 and 160 µg/mL), cells exhibited morphological changes such as rounding, cytoplasmic condensation, reduced adherence, partial detachment, and decreased cell density, indicating concentration-dependent cellular damage. These observations were consistent with the MTT assay, which demonstrated reduced cell viability at higher NPs concentrations.

The observed concentration-dependent morphological alterations may be associated with intracellular ROS generation and Zn^{2+} ion release from ZnO nanoparticles, resulting in oxidative stress, cytoskeletal disruption, and early apoptotic events. The comparatively mild morphological changes observed at lower concentrations suggest that the PVP coating and *Adiantum capillus-veneris* phytochemicals improved nanoparticle dispersion and reduced direct nanoparticle–cell interactions, thereby enhancing cytocompatibility (Wang *et al.* 2015). Similar morphological responses, including cell shrinkage, rounding, reduced adhesion, and cytoskeletal alterations following ZnO nanoparticle exposure, have been reported in mammalian cells and were attributed to ROS-mediated oxidative stress (Pinho *et al.* 2020). Likewise, ACV extracts have been reported to exhibit dose-dependent effects on cell morphology and viability due to their bioactive compounds (Roy *et al.* 2019). Overall, the morphological analysis confirms that ACV-Zn@PVP nanoparticles exhibit good cellular compatibility at lower concentrations while inducing moderate morphological alterations only at higher concentrations.

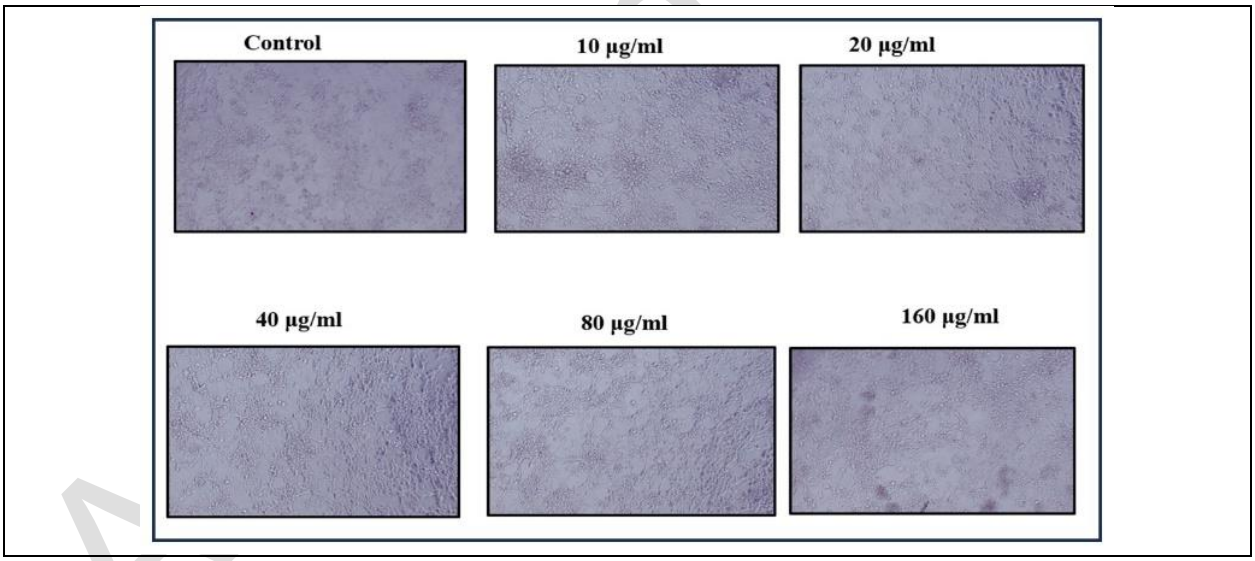

Fig. 9: Phase-contrast microscopic images showing the morphological changes of V79 fibroblast cells after treatment with ACV-Zn@PVP NPs at concentrations of control, 10, 20, 40, 80, and 160 µg/mL for 24 h

4. CONCLUSION

In the present study, *Adiantum capillus-veneris*-functionalized PVP-coated zinc oxide nanoparticles (ACV-Zn@PVP NPs) were successfully synthesized using a simple, eco-friendly, and cost-effective one-pot green synthesis approach. The phytochemicals present in the aqueous leaf extract served as natural reducing and stabilizing agents, while PVP effectively enhanced nanoparticle stability and minimized aggregation. The successful formation of ACV-Zn@PVP NPs was confirmed through UV–Visible spectroscopy, FTIR, FESEM-EDX, XRD, DLS, and zeta potential analyses, demonstrating the formation of crystalline, phase-pure, and colloidally stable ZnO nanoparticles. The synthesized nanoparticles exhibited concentration-dependent antibacterial activity against both Gram-positive and Gram-negative bacterial pathogens, with the greatest inhibition observed against *Escherichia coli* and *Klebsiella pneumoniae*. In addition, the MTT assay and

morphological evaluation demonstrated good cytocompatibility toward normal V79 fibroblast cells at lower concentrations, while only moderate concentration-dependent effects were observed at higher concentrations. These findings indicate that ACV-Zn@PVP nanoparticles possess favorable physicochemical characteristics, effective antibacterial activity, and acceptable in vitro cytocompatibility.

However, the present study has several limitations. The biological evaluation was restricted to in vitro antibacterial assays and cytocompatibility assessment using a single normal cell line. The underlying antibacterial and cellular mechanisms, including reactive oxygen species (ROS) generation, were not experimentally investigated, and antibiofilm activity, molecular mechanisms, long-term colloidal stability, and in vivo biocompatibility were beyond the scope of this work. Therefore, future studies should focus on investigating ROS-mediated antibacterial mechanisms, antibiofilm efficacy, gene and protein expression associated with oxidative stress and bacterial cell death, long-term physicochemical stability, evaluation using clinically relevant infection models, and comprehensive in vivo biocompatibility studies. Furthermore, the excellent colloidal stability and cytocompatibility observed in the present study suggest that ACV-Zn@PVP nanoparticles may be explored in future as potential carriers for drug delivery and other antimicrobial biomedical applications after extensive preclinical validation.

AUTHOR CONTRIBUTIONS

Devadharshini: Conceptualization, Methodology, Investigation, Writing – original draft. G. Pallavi: Validation, Formal analysis, Data curation, Software. S. Revathi: Supervision, Project administration, Resources, Funding acquisition, Writing – review & editing. All authors have read and agreed to the published version of the manuscript.

Availability of Data and Materials

All data generated or analyzed during this study are included in this published article.

ACKNOWLEDGMENT

The authors thank the management of SIMATS, Chennai, for providing the necessary infrastructure and support to carry out this research work.

FUNDING

This research received no specific grant from any funding agency in the public, commercial, or not-for-profit sectors.

CONFLICTS OF INTEREST

The authors declare that there is no conflict of interest.

COPYRIGHT

REFERENCE

Abdolalian, S. and Taghavijeloudar, M., Performance evaluation and optimization of ZnO-PVP nanoparticles for photocatalytic wastewater treatment: Interactions between UV light intensity and nanoparticles dosage, *J. Clean. Prod.*, 365, 132833 (2022). https://doi.org/10.1016/j.jclepro.2022.132833

AboGabal, R., Shokeir, D. and Oraby, A. H., Design and synthesis of biologically inspired biocompatible various polymeric magnetic nanoparticles for imaging and biomedical applications, *Nano-Struct. Nano-Obj.*, 36, 101048 (2023). https://doi.org/10.1016/j.nanoso.2023.101048

Ahmed, S. K., Hussein, S., Qurbani, K., Ibrahim, R. H., Fareeq, A., Mahmood, K. A. and Mohamed, M. G., Antimicrobial resistance: Impacts, challenges, and future prospects, *J. Med. Surgery Pub. Hea.*, 2, 100081 (2022). https://doi.org/10.1016/j.glmedi.2024.100081

Alanazi, M. M., Biomedical potential, optical properties, and morphological features of green-synthesized silver nanoparticles using *Acacia nilotica* fruit extract under visible light, *J. Taibah Univers. Sci.*, 19(1) 2554023(2025). https://doi.org/10.1080/16583655.2025.2554023

Ali, S. A., Osman, M. E. and Mohamed, E. T., Eco-friendly biosynthesis of silver nanoparticles using marine-derived Fusarium exquisite: optimization, characterization, and evaluation of antimicrobial, antioxidant, and cytotoxic activities, *World J. Microbio. Biotechnol.*, 41(5), 165 (2025). https://doi.org/10.1007/s11274-025-04368-w

Ansari, M. A., Murali, M., Prasad, D., Alzohairy, M. A., Almatroudi, A., Alomary, M. N., Udayashankar, A. C., Singh, S. B., Asiri, S. M. M., Ashwini, B. S., Gowtham, H. G., Kalegowda, N., Amruthesh, K. N., Lakshmeesha, T. R. and Niranjana, S. R., Cinnamomum verum bark extract mediated green synthesis of ZnO nanoparticles and their antibacterial potentiality, *Biomol.*, 10(2), E336 (2020). https://doi.org/10.3390/biom10020336

Baliyan, S., Mukherjee, R., Priyadarshini, A., Vibhuti, A., Gupta, A., Pandey, R. P. and Chang, C. M., Determination of antioxidants by DPPH radical scavenging activity and quantitative phytochemical analysis of Ficus religiosa, *Mol.*, 27(4), 1326 (2022). https://doi.org/10.3390/molecules27041326

Dehdari, S. and Hajimehdipoor, H., Medicinal properties of *Adiantum capillus-veneris* Linn. In traditional medicine and modern phytotherapy: A review article, *Iran. J. Pub. Health*, 47(2), 188–197 (2018). https://www.ncbi.nlm.nih.gov/pubmed/29445628

Dheyab, M. A., Aziz, A. A., Nowfal, S. H., Braim, F. S., Abdullah, W., Kasasbeh, W. H., Jameel, M. S., Alanezi, S. T., Alrosan, M. and Oladzadabbasabadi, N., Sustainable green synthesis of silver nanoparticles for safer biomedical application, *J. Environ. Chem. Eng.*, 13(2), 115998 (2025). https://doi.org/10.1016/j.jece.2025.115998

Diab, M., Jadhav, A. H. and Alwarsamy, M., The synergistic effect of biosynthesized silver nanoparticles from a combined extract of Petroselinum crispum and Piper betle: in vitro antibacterial activity, *Res. Chem.*, 18, 102816 (2025). https://doi.org/10.1016/j.rechem.2025.102816

Ebrahimzadeh, M., Rahbari, S., Doust, R. H. and Mojab, F., In vitro antibacterial activity of Adiantum capillus veneris extraction with methanol, chloroform, and ether solvents against Methicillin-resistant *Staphylococcus aureus*, *Curr. Drug Discovery Technol.*, 22(4), e15701638313570 (2024). https://doi.org/10.2174/0115701638313570241015045118

El-Saadony, M. T., Fang, G., Yan, S., Alkafaas, S. S., El Nasharty, M. A., Khedr, S. A., Hussien, A. M., Ghosh, S., Dladla, M., Elkafas, S. S., Ibrahim, E. H., Salem, H. M., Mosa, W. F. A., Ahmed, A. E., Mohammed, D. M., Korma, S. A., El-Tarabily, M. K., Saad, A. M., El-Tarabily, K. A. and AbuQamar, S. F., Green synthesis of zinc oxide nanoparticles: Preparation, characterization, and biomedical applications - A review, *Int. J. Nanomed.*, 19, 12889–12937 (2024). https://doi.org/10.2147/IJN.S487188

Elshobary, M. E., Badawy, N. K., Ashraf, Y., Zatioun, A. A., Masriya, H. H., Ammar, M. M., Mohamed, N. A., Mourad, S. and Assy, A. M., Combating antibiotic resistance: Mechanisms, multidrug-resistant pathogens, and novel therapeutic approaches: An updated review, *Pharma. (Basel, Switzerland)*, 18(3), 402 (2025). https://doi.org/10.3390/ph18030402

Franco, P. and De Marco, I., The use of poly(N-vinyl pyrrolidone) in the delivery of drugs: A review, *Polym.*, 12(5), E1114 (2020). https://doi.org/10.3390/polym12051114

Harun-Ur-Rashid, M., Foyez, T., Krishna, S. B. N., Poda, S. and Imran, A. B., Recent advances of silver nanoparticle-based polymer nanocomposites for biomedical applications, *RSC Adv.*, 15(11), 8480–8505 (2025). https://doi.org/10.1039/d4ra08220f

Ibraheim, Z. Z., Ahmed, A. S. and Gouda, Y. G., Phytochemical and biological studies of *Adiantum capillus-veneris* L, *Saudi Pharma. J.*, 19(2), 65–74 (2011). https://doi.org/10.1016/j.jsps.2011.01.007

Ihsan, M., Din, I. U., Alam, K., Munir, I., Mohamed, H. I. and Khan, F., Green fabrication, characterization of zinc oxide nanoparticles using plant extract of Momordica charantia and Curcuma zedoaria and their antibacterial and antioxidant activities, *Appl. Biochem. Biotechnol.*, 195(6), 3546–3565 (2023). https://doi.org/10.1007/s12010-022-04309-5

Irma, M. B. and Žujo., The review on the antimicrobial potential of Maidenhair fern, *Adiantum capillus-veneris* L. *Annals Institute Bio. Univers. Sarajevo*, 45, 41–58 (2023). https://doi.org/10.35666/2831-0705.2023.45.41

Ishaq, M. S., Hussain, M. M., Afridi, M. S., Ali, G., Khattak, M., Ahmad, S. and Shakirullah., In vitro phytochemical, antibacterial, and antifungal activities of leaf, stem, and root extracts of Adiantum capillus veneris, *Sci. World J.*, 2014, 269793 (2014). https://doi.org/10.1155/2014/269793

Jebahi, S., Badraoui, R., Ben Salah, G., Ben Taheur, F., Brahmi, F., Mhadhbi, M., Bouhamda, T., Jilani, S., Aloufi, B., Adnan, M., Siddiqui, A. J., Sulieman, A. M. E. and Karmous, I., Green synthesis of plant-derived ZnO nanoparticles: Characterization, pharmacokinetics, molecular interactions, and in-vitro antimicrobial and antifungal evaluation, *Biomol. Biomed.*, 25(10), 2378–2393 (2025). https://doi.org/10.17305/bb.2025.12090

Karampour, F., Green synthesis and characterization of ZnO nanoparticles from Echinophora platyloba DC. Extract and HSA interaction study, *Asian J. Green Chem.*, 7(3), 149–162 (2023). https://doi.org/10.22034/ajgc.2023.394268.1384

Kazemi, S., Hosseingholian, A., Gohari, S. D., Feirahi, F., Moammeri, F., Mesbahian, G., Moghaddam, Z. S. and Ren, Q., Recent advances in green synthesized nanoparticles: from production to application, *Mater. Today Sustain.*, 24, 100500 (2023). https://doi.org/10.1016/j.mtsust.2023.100500

Kim, O., Kwon, J., Kim, S., Xu, B., Seo, K., Park, C., Do, W., Bae, J. and Kang, S., Effect of PVP-capped ZnO nanoparticles with enhanced charge transport on the performance of P3HT/PCBM polymer solar cells, *Polym.*, 11(11), E1818 (2019). https://doi.org/10.3390/polym11111818

Kiran, K. D. and Kumar, D., Synthesis of zinc oxide nanoparticles using dark chocolate and its anti-inflammatory activity, *Int. J. Drug Delivery Technol.*, 16(62s) (2026). https://doi.org/10.25258/ijddt.16.62s.9

Mesbah, F., El Gayar, D., Farag, H., Tamer, T. M., Omer, A. M., Mohy-Eldin, M. S. and Khalifa, R. E., Development of highly ionic conductive cellulose

acetate-g-poly (2-acrylamido-2-methylpropane sulfonic acid-co-methyl methacrylate) graft copolymer membranes, *J. Saudi Chem. Soc.*, 25(9), 101318 (2021). https://doi.org/10.1016/j.jscs.2021.101318

Mohammed, A. M., Mohammed, M., Oleiwi, J. K., Ihmedee, F. H., Adam, T., Betar, B. O. and Gopinath, S. C. B., Comprehensive review on zinc oxide nanoparticle production and the associated antibacterial mechanisms and therapeutic potential, *Nano Trends*, 11, 100145 (2025). https://doi.org/10.1016/j.nwnano.2025.100145

Namvar, F., Rahman, H. S., Mohamad, R., Azizi, S., Tahir, P. M., Chartrand, M. S. and Yeap, S. K., Cytotoxic effects of biosynthesized zinc oxide nanoparticles on murine cell lines, *Evidence-Based Complement. Alternat. Med.*, 2015, 593014 (2015). https://doi.org/10.1155/2015/593014

Nazim, M. D., Aslam, M. and Chaudhary, S. S., HANSRAJ (*Adiantum capillus-veneris*) -A REVIEW, *J. Drug Delivery Therap.*, 8(5-s), 105–109 (2018). https://doi.org/10.22270/jddt.v8i5-s.2065

Olejnik, M., Kersting, M., Rosenkranz, N., Loza, K., Breisch, M., Rostek, A., Prymak, O., Schürmeyer, L., Westphal, G., Köller, M., Bünger, J., Epple, M. and Sengstock, C., Cell-biological effects of zinc oxide spheres and rods from the nano- to the microscale at sub-toxic levels, *Cell Bio. Toxicol.*, 37(4), 573–593 (2021). https://doi.org/10.1007/s10565-020-09571-z

Omidi, S., Sedaghat, S., Tahvildari, K., Derakhshi, P. and Motiee, F., Biosynthesis of silver nanoparticles with *Adiantum capillus-veneris* L leaf extract in the batch process and assessment of antibacterial activity, *Green Chem. Lett. Rev.*, 11(4), 544–551(2018). https://doi.org/10.1080/17518253.2018.1546410

Parvin, N., Joo, S. W. and Mandal, T. K., Nanomaterial-based strategies to combat antibiotic resistance: Mechanisms and applications, *Antibio.*, 14(2), 207 (2025). https://doi.org/10.3390/antibiotics14020207

Pathak, K., Sarma, M., Sahariah, M., Shankarishan, P., Sahariah, J. J., Deka, S., Das, A., Islam, M. A., Pramanik, P., Borthakur, P. P., Bharadwaj, A. R. and Bhaumik, R., Nanoparticles in the fight against antimicrobial challenges: A comprehensive review, *Next Nanotechnol.*, 9, 100420 (2026). https://doi.org/10.1016/j.nxnano.2026.100420

Pinho, A. R., Martins, F., Costa, M. E. V., Senos, A. M. R., Silva, O. A. B. da C. E., Pereira, M. de L. and Rebelo, S., In vitro cytotoxicity effects of zinc Oxide Nanoparticles on spermatogonia cells, *Cells*, 9(5), E1081 (2020). https://doi.org/10.3390/cells9051081

Qadir, S. A., Awlqadr, F. H., Qadir, M. H., Qadir, A. M., Faraj, A. M., Salih, S. A., Saeed, M. N., Arab, K. and Hosseini, S. M. N., *Adiantum capillus-veneris*: A comprehensive review of its medicinal properties, bioactive compounds, and advanced extraction techniques, *Food Sci. Nutri.*, 13(10), e71118 (2025). https://doi.org/10.1002/fsn3.71118

Ragavendran, C., Kamaraj, C., Alam, M. W. and Rajkumar, M., Eco-friendly synthesis of zinc oxide nanoparticles using Caralluma adscendens stem extract: Characterization, antibacterial, antioxidant, and cytotoxic effects of breast cancer cells, *Inorg. Chem. Commun.*, 180, 115035 (2025). https://doi.org/10.1016/j.inoche.2025.115035

Ramnandan, D., Mokhosi, S., Daniels, A. and Singh, M., Chitosan, polyethylene glycol and polyvinyl alcohol modified $MgFe_2O_4$ ferrite magnetic nanoparticles in doxorubicin delivery: A comparative study in vitro, *Mol.*, 26(13), 3893 (2021). https://doi.org/10.3390/molecules26133893

Roy, S. C., Sajeeb, B. K., Muhit, M. A. and Bachar, S. C., Evaluation of antioxidant and cytotoxic activities of aerial parts of *Adiantum capillus-veneris* L. growing in Bangladesh, *Dhaka Univers. J. Pharma. Sci.*, 18(2), 217–222 (2019). https://doi.org/10.3329/dujps.v18i2.43264

Safo, I. A., Werheid, M., Dosche, C. and Oezaslan, M., The role of polyvinylpyrrolidone (PVP) as a capping and structure-directing agent in the formation of Pt nanocubes, *Nanoscale Adv.*, 1(8), 3095–3106 (2019). https://doi.org/10.1039/c9na00186g

Salam, M. A., Al-Amin, M. Y., Salam, M. T., Pawar, J. S., Akhter, N., Rabaan, A. A. and Alqumber, M. A. A., Antimicrobial resistance: A growing serious threat for global public health, *Healthcare*, 11(13), 1946 (2023). https://doi.org/10.3390/healthcare11131946

Santhoshkumar, J., Kumar, S. V. and Rajeshkumar, S., Synthesis of zinc oxide nanoparticles using plant leaf extract against urinary tract infection pathogen, *Resource-Efficient Technol.*, 3(4), 459–465 (2017). https://doi.org/10.1016/j.reffit.2017.05.001

Sayeem, N. R., Podder, U., Alam, M. A., Shishir, M. K. H., Miah, M. A. R., Anik, F. K., Ghosh, P., Ahmed, S., Islam, M. and Jahan, S. A., Critical perspective review on green synthesis of zinc oxide nanoparticles: Explored wurtzite phase, characterization and real world applications, *Next Nanotechnol.*, 9, 100412 (2026). https://doi.org/10.1016/j.nxnano.2026.100412

Shanmugam, N., Dhanaraj, K., Viruthagiri, G., Balamurugan, K. and Deivam, K., Synthesis and characterization of surfactant assisted Mn^{2+} doped ZnO nanocrystals, *Arab. J. Chem.*, 9, S758–S764 (2016). https://doi.org/10.1016/j.arabjc.2011.08.016

Singh, K., Nancy, Bhattu, M., Singh, G., Mubarak, N. M. and Singh, J., Light-absorption-driven photocatalysis and antimicrobial potential of PVP-capped zinc oxide nanoparticles, *Sci. Rep.*, 13(1), 13886 (2023). https://doi.org/10.1038/s41598-023-41103-7

Sirelkhatim, A., Mahmud, S., Seeni, A., Kaus, N. H. M., Ann, L. C., Bakhori, S. K. M., Hasan, H. and

Mohamad, D., Review on zinc oxide nanoparticles: Antibacterial activity and toxicity mechanism, *Nano-Micro Lett.*, 7(3), 219–242 (2015). https://doi.org/10.1007/s40820-015-0040-x

Suciyati, S. W., Manurung, P., Junaidi, J. and Situmeang, R., Optical and crystal structure properties of ZnO nanoparticle synthesized through biosynthesis method for photocatalysis application, *Indones. J. Chem.*, 24(1), 125 (2024). https://doi.org/10.22146/ijc.84796

Surya, M., Mohanta, Y. K., Mohammedsaleh, Z. M., Sankar, M., Panneerselvam, C., Savariar, V. and Saravanan, M., Eco-friendly synthesis of Ag/ZnO nanocomposite using Coleus amboinicus: Structural characterization and evaluation of antibacterial and anticancer activities, *Next Nanotechnol.*, 9, 100334 (2026). https://doi.org/10.1016/j.nxnano.2025.100334

Teodorescu, M. and Bercea, M., Poly(vinylpyrrolidone) – A versatile polymer for biomedical and beyond medical applications, *Polym. Plast. Technol. Eng.*, 54(9), 923–943 (2015). https://doi.org/10.1080/03602559.2014.979506

Thakur, K. and Kaur, A., Hibiscus rosa-sinensis flower extract-mediated fabrication of zinc oxide nanoparticles, characterization and its antimicrobial activity, *Pharmacol. Res. Modern Chinese Med.*, 16, 100673 (2025). https://doi.org/10.1016/j.prmcm.2025.100673

Tu, W.-X., Zuo, X.-B. and Liu, H.-F., Study on the interaction between polyvinylpyrrolidone and platinum metals during the formation of the colloidal metal nanoparticles. *Chinese Journal of Polymer Science*, 26(01), 23 (2008). https://doi.org/10.1142/s0256767908002625

Unni, V., Abishad, P., Arya, P. R., Mohan, B., Juliet, S., John, L., Nambiar, P., Vinod, V. K., Karthikeyan, A., Kurkure, N. V., Barbuddhe, S. B., Rawool, D. B. and Vergis, J., Eco-friendly one pot synthesis of zinc oxide nanoparticles using catkin extract of Piper longum: In vitro antibacterial, antioxidant and antibiofilm potential against multi drug resistant enteroaggregative *E. coli*, *2nd Int. Electron. Conf. Biomed.*, 14 (2023). https://doi.org/10.3390/ecb2023-14269

Vantipalli, R. S. H., Ilangovar, I. G. K., Vasugi, S. and Sivaperumal, P., Synthesis of zinc oxide nanoparticles from Cymodocea serrulata leaf extract and their biological activities, *Cureus*, 16(3), e55521 (2024). https://doi.org/10.7759/cureus.55521

Villagrán, Z., Anaya-Esparza, L. M., Velázquez-Carriles, C. A., Silva-Jara, J. M., Ruvalcaba-Gómez, J. M., Aurora-Vigo, E. F., Rodríguez-Lafitte, E., Rodríguez-Barajas, N., Balderas-León, I. and Martínez-Esquivias, F., Plant-based extracts as reducing, capping, and stabilizing agents for the Green synthesis of inorganic nanoparticles, *Res.*, 13(6), 70 (2024). https://doi.org/10.3390/resources13060070

Wang, C., Hu, X., Gao, Y. and Ji, Y., ZnO nanoparticles treatment induces apoptosis by increasing intracellular ROS levels in LTEP-a-2 cells, *BioMed Res. Int.*, 2015, 423287 (2015). https://doi.org/10.1155/2015/423287

Yagnik, D., Serafin, V. and J Shah, A., Antimicrobial activity of apple cider vinegar against *Escherichia coli*, *Staphylococcus aureus* and Candida albicans; downregulating cytokine and microbial protein expression, *Sci. Rep.*, 8(1), 1732 (2018). https://doi.org/10.1038/s41598-017-18618-x